Proceedings of the 21st ICSMGE, Vienna, Austria, 14 – 19 June 2026. Pistrol, Adam & Schweiger (eds.)
Published by: ÖGG, Austrian Society for Geomechanics, Salzburg, Austria, ISBN 978-3-9503898-4-5
https://doi.org/10.53243/ICSMGE2026-820

MT-InSAR monitoring of deep excavations: a feasibility study of analytical kinematic constraints to assess three-dimensional surface movements

Adriana Hernandez-Guardado, Andrea Franza
Department of Civil and Architectural Engineering, Aarhus University, Denmark, adriana.hernandez@cae.au.dk.

Diego Reale
Institute for Electromagnetic Sensing of the Environment, National Research Council of Italy (CNR-IREA), Naples, Italy.

Gianfranco Nicodemo, Dario Peduto
Department of Civil Engineering, University of Salerno, Fisciano, Italy.

Francesco Petrella
Ove Arup & Partners Danmark A/S, Copenhagen, Denmark.

ABSTRACT: Multi-temporal Interferometric Synthetic Aperture Radar (MT-InSAR) has become a valuable tool for monitoring surface movements in urban areas. This study integrates MT-InSAR data from complementary ascending and descending orbits, with kinematic analytical constraints to evaluate three-dimensional ground displacements induced by deep excavations. A case study of metro station construction in Copenhagen's Cityringen is presented, where ground movements were induced by piling and excavation activities. To assess the reliability of MT-InSAR against terrestrial benchmarks, displacement time series from very-high-resolution X-band satellites (TerraSAR-X and Cosmo-SkyMed) are compared with three-dimensional terrestrial measurements. A novel method is then introduced that integrates dual-orbit MT-InSAR measurements with an analytical kinematic model to assess 3D displacement directions, grounded in the physical behaviour of deep excavations. This allows for decomposition of satellite observations along the radar Line-of-Sight (LOS) into vertical and horizontal components around a rectangular excavation. A study of the directional sensitivity of Analytically Constrained InSAR (AC-InSAR) to the variance of LOS measurements is carried out. Finally, the kinematically constrained MT-InSAR results are compared with terrestrial data to demonstrate the feasibility and accuracy of the proposed approach.

KEYWORDS: MT-InSAR, monitoring, ground displacements, deep excavations, analytical model.

INTRODUCTION

Monitoring and back-analysis of ground movements induced by excavations are essential for managing risks in dense urban settings and improving prediction methods. Figure 1 illustrates the wall deflections and ground movements for a rectangular deep excavation (e.g. metro station box), which are inherently three-dimensional (3D) due to the complex interplay between the excavation and construction sequence, support systems, and ground.

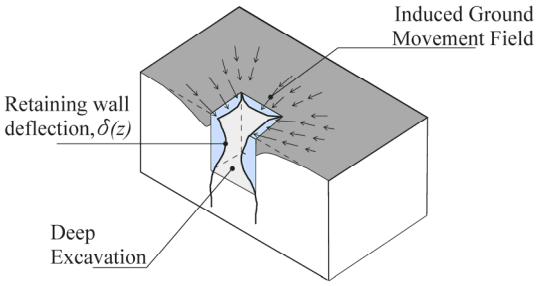

Figure 1. Considered problem: rectangular deep excavation.

In this context, Multi-Temporal Interferometric Synthetic Aperture Radar (MT-InSAR) has emerged as a valuable remote sensing technology, capable of detecting surface displacements with millimetre-level accuracy over wide areas (Peduto et al., 2025). For infrastructure and urban monitoring, MT-InSAR has been successfully applied in various geotechnical contexts, including slow-moving landslides (Noviello et. al., 2020), subsidence (Peduto et al., 2019) and tunnelling (Giardina et al., 2019; De Luca et al., 2024). However, its application to 3D excavations is challenging. Conventional MT-InSAR techniques are limited to measuring displacements along the satellite radar Line-of-Sight (LOS), which is not adequate to quantify 3D excavation-induced displacement fields, particularly when displacements have horizontal components in both the East and North directions. This limitation arises because current satellite SAR missions operate on quasi-polar orbits, resulting in poor sensitivity to the North-South components of ground movement.

Previous studies have combined LOS measurements from complementary ascending and descending orbits to estimate two-dimensional displacement fields, usually through the estimation of West-East and Vertical components, relying on assumptions such as plane-strain conditions or negligible north-south displacements (Ritter et al. 2021), which may introduce errors (Brouwer and Hanssen, 2023). To overcome these shortcomings, Brouwer and Hanssen (2024) proposed the "strapdown" approach for 3D displacements estimation, which introduces the expected deformation direction as *a priori* physically informed constraint. While this approach has been successfully applied to landslides and linear infrastructure monitoring (Cascini et al., 2010; Chang et al., 2018; Solarte et al., 2025), its use in 3D excavation scenarios in urban areas remains underexplored. Thus, tailoring strapdown approaches for 3D excavations is relevant.

This paper proposes a novel methodology, referred to as Analytically Constrained InSAR (AC-InSAR) deformation analysis, to study 3D excavation-induced displacement fields (e.g. metro station construction). It combines the analysis of dual-orbit MT-InSAR ascending and descending datasets, with an analytical kinematic constraint model of the horizontal total displacement direction (accounting for the correlation between underground construction and a salient feature of the surface deformation field). First, the case study of the Skjolds Plads

(SKP) metro station construction during the Cityringen project in Copenhagen is presented, including a comparison of selected terrestrial instrumentation and MT-InSAR measurements along the satellite alignments. Second, the theoretical framework of the proposed AC-InSAR method is detailed, along with a study of expected performance depending on the horizontal displacement vector orientation. Finally, for the case study, 3D displacements predicted from the AC-InSAR and terrestrial instrumentation are compared as proof-of-concept application.

1 DATASETS AND CASE STUDY

This study uses Synthetic Aperture Radar (SAR) datasets acquired from the COSMO-SkyMed (CSK) and TerraSAR-X (TSX) satellite missions. Both systems operate in the X-band and provide very high-resolution radar imagery (i.e. with a ground spatial resolution of ~3m in standard Stripmap acquisition mode).

Both datasets have been processed at the full available resolution for the detection of Persistent Scatterers (PS). Specifically, the CSK dataset (96 descending-orbit images, acquired between Apr-2011 and Dec-2019, beam H4-01 corresponding to an incidence angle (θ) at scene centre of ~26.2° and heading angle $\alpha = 347.7°$) was processed by CNR-IREA using the SAR Tomography technique (Fornaro et al., 2014). On the other hand, the TSX dataset (176 ascending-orbit images, acquired between Sept-2011 and May-2020, track 55A, beam strip_013, $\theta \approx 42.8°$ and $\alpha = 350.3°$) was processed by DTU Space using the Persistent Scatterer SAR Interferometry (PS-InSAR) algorithm implemented in the *SAPROZ* software (Styrelsen for Dataforsygning og Effektivisering, 2022).

The Cityringen metro line (M3) is a circular underground metro system in central Copenhagen, comprising 17 stations, two crossovers, and three shaft structures (Olbekk et al., 2022). This study focuses on SKP, one of the station boxes constructed as part of the M3 line, which was built between Dec-2011 to Dec-2015. Figure 2 shows the alignment of the M3 line in the city centre of Copenhagen, Denmark, and the location of SKP. Construction followed a hybrid bottom-up method. In this approach, the central part of the permanent roof slab was cast before excavation began. Then, the excavation was supported by temporary secant piles and temporary tubular struts. The base slab was cast upon reaching the final excavation depth, and the temporary supports were removed as the intermediate, technical, and concourse slabs were constructed (Olbekk et al., 2022).

Figure 2. Skjolds Plads (SKP) location and Cityringen alignment.

The geological profile at SKP consists of fill, glacial soils (clay till, meltwater sand) and Upper Copenhagen limestone, encountered at approximately 19 m below ground level ($H_l = 19\ m$). Ground displacements were observed in the surrounding area throughout the entire construction process, including secant pile wall installation (boring and casting), excavation, and construction of permanent structures.

Horizontal ground movements ranging between 10 and 12.5 mm were recorded near the retaining walls, primarily induced by piling and excavation activities, while settlements reached values up to 10 mm. To evaluate the accuracy of satellite-based displacement measurements, MT-InSAR datasets (Figure 3) are compared with terrestrial monitoring data (Figure 5). As benchmarks for the AC-InSAR measurements, this study uses measurements from a 3D automated total station installed on nearby buildings (approx. 11 m above ground) with an accuracy of ±1 mm.

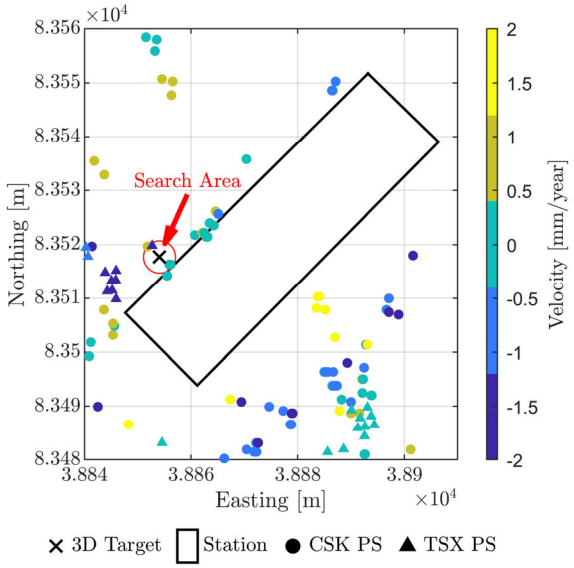

Figure 3. Plan locations of measurements at SKP station: persistent scatterers (colour-coded for LOS velocity) and 3D target.

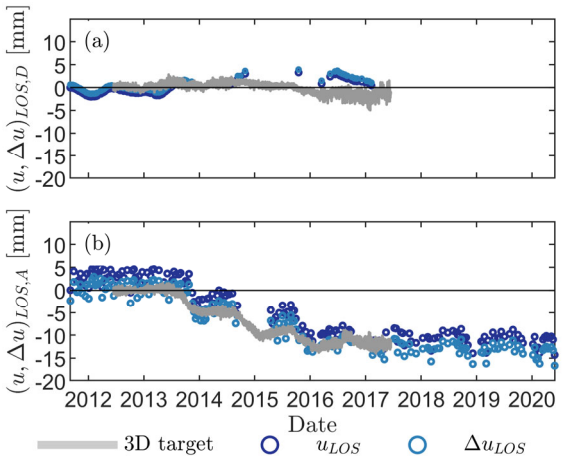

Figure 4. Comparison between MT-InSAR and terrestrial data projected on LOSs: (a) descending CSK, (b) ascending TSX.

Figure 3 shows the spatial distribution of PS from CSK and TSX processing and the location of the terrestrial monitoring (referred to as "*3D target*"), located approximately 2.5 m behind the retaining wall and at 11.3 m above ground level near the west corner of the station box; in addition, this figure displays a 6 m diameter region centred at the 3D target, which is used as a search zone of nearby permanent scatters to ensure proximity between ascending and descending measurements. In

terms of measured displacement histories (i.e. displacement–time curves), Figure 4 shows the projection of the 3D target displacements onto each of the satellites' LOS in the ascending and descending orbits. The figure shows both the satellite's "*LOS measurement*" u_{LOS} as well as the "*offset LOS measurement*" $\Delta u_{los} = u_{LOS} - u_{LOS,avg}$ defined relative to a baseline, which is $u_{LOS,avg}$ equal to the average of u_{LOS} during its first year. Both projected 3D target and LOS MT-InSAR displacements along the descending orbit alignment (i.e. from $\theta = 26.2°$ and $\alpha = 347.7°$) fluctuate around zero; at the 3D target location, this alignment has a limited sensitivity to excavation-induced movements that are predominantly horizontal. On the other hand, the TSX data capture both the magnitudes and temporal trends of the terrestrial ground movement along the ascending orbit alignment (i.e. from $\theta = 42.8°$ and $\alpha = 350.3°$), owing to a more favourable alignment with the displacement direction, as discussed in Section 3.

2 PROPOSED METHODOLOGY

2.1 *MT-InSAR Principles*

The InSAR measurements $u_{LOS,A}$ and $u_{LOS,D}$ correspond to the projection of the true displacement vector along the LOS, which can be arranged in a vector $\boldsymbol{u}_{LOS} = [u_{LOS,A}\, u_{LOS,D}]^T$. In the ENZ system, the global displacement vector is $\boldsymbol{u}_{gl} = [u_E\, u_N\, u_Z]^T$ where u_E, u_N, and u_Z are the components in the east, north, and vertical directions, respectively. Equations (1) and (2) describe the relationship between the LOS displacement $u_{LOS,i}$ and the true displacement $\boldsymbol{u}_{gl}$ through the unit vector $\boldsymbol{l}$ in the i-th orbit (Cascini et al., 2010). The components of $\boldsymbol{l}$ depend on the satellite's incidence θ and heading angle α.

$$u_{los,i} = \boldsymbol{l}_i^T \boldsymbol{u}_{gl} = u_E l_{E,i} + u_N l_{N,i} + u_Z l_{Z,i} \tag{1}$$

$$\begin{aligned} l_i^T &= [l_{E,i}\ \ l_{N,i}\ l_{Z,i}]^T \\ &= [-\sin\theta_i \cos\alpha_i\, , \sin\theta_i \sin\alpha_i\, , \cos\theta_i] \end{aligned} \tag{2}$$

When two viewing geometries are available, specifically ascending $u_{LOS,A}$ and descending $u_{LOS,D}$, the system of equations remains underdetermined. In this case, the full three-dimensional displacement vector $\boldsymbol{u}$ cannot be resolved using MT-InSAR data alone. This limitation becomes particularly relevant when the true horizontal displacement vector $\boldsymbol{u}_h$ is relatively large. To overcome this, models acting as kinematic constraints must be included to invert the problem (Brower and Hanssen 2023, Solarte et al. 2025) at the point of interest. The following section presents the analytical approach adopted in this study.

2.2 *Constraining of Double-Orbit MT-InSAR Data*

The assumption of the proposed Analytically Constrained InSAR (AC-InSAR) method is that the direction of the horizontal displacement $\boldsymbol{u}_h$ is known at every surface point around the excavation. This direction is therefore treated as a kinematic constraint within the InSAR system of equations and is defined by the angle ω, referred to as "*constraining angle*", which varies across the surface. This orientation is analytically prescribed as $\omega = \omega_{an}$, based on ground loss solutions (detailed in the next section). For validation purposes, the direction could also be obtained from field measurements, in which case $\omega = \omega_{field}$. In other words, AC-InSAR assumes that the displacement field at each point of interest (i) lies within a vertical plane inclined relative to a horizontal axis by an angle ω and (ii) within these planes the displacement field is described by a constrained vector $\boldsymbol{u}_\omega = [u_h\, u_z]^T$ with horizontal and vertical components u_h and u_z, respectively.

For deep rectangular excavations, Figure 5 shows in plan view the horizontal displacement vector $\boldsymbol{u}_h$ at a "*point of interest*". In the ENZ coordinate system, the angle between $\boldsymbol{u}_{h,gl} = [u_E\, u_N\,]^T$ and the East direction is denoted as ω_E. Alternatively, the local coordinate system (X, Y, Z) may be used where the horizontal axes are aligned with the excavation walls. In the local system, the horizontal displacement is expressed as $\boldsymbol{u}_{h,loc} = [u_x\, u_y\,]^T$ where u_x and u_y are the displacement components along the wall directions. The orientation of $\boldsymbol{u}_h$ relative to the local x-axis is denoted as $\omega_x(x, y)$. The angle between the local and global coordinate systems is β_a and is taken as positive anticlockwise; from definitions, $\omega_E = \beta_a + \omega_x$. While ω can be influenced by the geometry of the excavation and support conditions, in areas where plane strain conditions apply (typically along the axes of symmetry), u_h is perpendicular to the excavation walls.

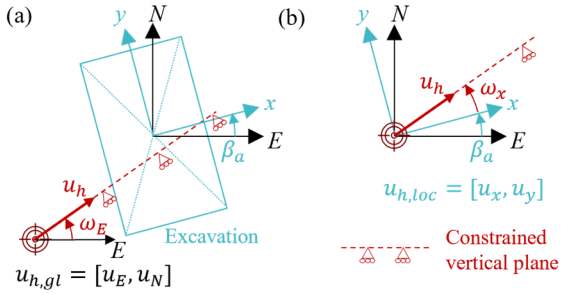

Figure 5. Plan view of the horizontal displacement: (a) in global (EZ) and (b) the local (XY) coordinate systems.

Next, the set of equations defining the AC-InSAR method is derived to show how the displacement vector, expressed as $\boldsymbol{u}_{gl} = [u_E\, u_N\, u_Z]^T$ or in a local system as $\boldsymbol{u}_{loc} = [u_x\, u_y\, u_Z]^T$, when constrained to lie in a vertical plane identified by the constraining angle ω, can be fully described using only two unknown scalar quantities: horizontal u_h and vertical u_z components of $\boldsymbol{u}_\omega$. Assuming that angles are measured as positive in the anticlockwise direction, it follows from the definitions that

$$\omega_E = \tan^{-1}\left(\frac{u_N}{u_E}\right);\ \ \omega_x = \tan^{-1}\left(\frac{u_y}{u_x}\right) \tag{3}$$

$$u_N = \frac{sin\omega_E}{cos\omega_E} u_E\ ;\ u_y = \frac{sin\omega_x}{cos\omega_x} u_x \tag{4}$$

In the ENZ frame, the LOS displacement measurements from both ascending (A) and descending (D) satellite passes ($u_{LOS,A}$ and $u_{LOS,D}$, respectively) can be related to true displacement components with this system of equations

$$\begin{bmatrix} u_{LOS,A} \\ u_{LOS,D} \end{bmatrix} = \begin{bmatrix} l_{E,A} & l_{N,A} & l_{Z,A} \\ l_{E,D} & l_{N,D} & l_{Z,D} \end{bmatrix} \begin{bmatrix} u_E \\ u_N \\ u_Z \end{bmatrix};$$

$$\boldsymbol{u}_{LOS} = \boldsymbol{L}\, \boldsymbol{u}_{gl} \tag{5}$$

Substituting Equation (4) into the system of Equation (5) eliminates the north component u_N as an independent variable. This leads to the constrained system shown in Equation (6) that is a determined set of equations when ω_E is (analytically) known, with $\boldsymbol{L}_C$ being the constrained transformation matrix between InSAR measurement and displacements (e.g. $\boldsymbol{L}_{C,an}$ corresponds to $\omega_E = \omega_{E,an}$).

$$\begin{bmatrix} u_{LOS_A} \\ u_{LOS_D} \end{bmatrix} = \begin{bmatrix} l_{E,A} + \dfrac{sin\omega_E}{cos\omega_E} l_{N,A} & l_{Z,A} \\ l_{E,D} + \dfrac{sin\omega_E}{cos\omega_E} l_{N,D} & l_{Z,D} \end{bmatrix} \begin{bmatrix} u_E \\ u_Z \end{bmatrix}; \quad (6)$$

$$\boldsymbol{u}_{LOS} = \boldsymbol{L}_C \begin{bmatrix} u_E \\ u_Z \end{bmatrix}$$

Equation (6) can be expressed in terms of the displacement vector within the constrained plane $\boldsymbol{u}_\omega = [u_h\ u_z]^T$ obtaining the final Eq. (7) in which the transformation matrix between LOS measurements and the constrained in-plane displacement components is described by the matrix $\boldsymbol{L}_{C,\omega}$:

$$\begin{bmatrix} u_{LOS,A} \\ u_{LOS,D} \end{bmatrix} = \begin{bmatrix} l_{E,A}cos\omega_E + l_{N,A}sin\omega_E & l_{Z,A} \\ l_{E,D}cos\omega_E + l_{N,D}sin\omega_E & l_{Z,D} \end{bmatrix} \begin{bmatrix} u_h \\ u_Z \end{bmatrix} \quad (7)$$

$$\boldsymbol{u}_{LOS} = \boldsymbol{L}_{C,\omega}\, \boldsymbol{u}_\omega$$

To facilitate interpretation relative to the excavation geometry by analysing $\boldsymbol{u}_{loc}$, a coordinate transformation is applied using a rotation matrix $\boldsymbol{R}_{rot}$, as proposed by Chang et al. (2018).

$$\boldsymbol{u}_{loc} = \boldsymbol{R}_{rot}\, \boldsymbol{u}_{gl}\ ;\ \ \boldsymbol{R}_{rot} = \begin{bmatrix} \cos\beta_a & \sin\beta_a & 0 \\ -\sin\beta_a & \cos\beta_a & 0 \\ 0 & 0 & 1 \end{bmatrix} \quad (8)$$

The spatial distribution of ω_E as a function of position (E, N) has been derived empirically (e.g. by Ritter et al., 2021) assuming horizontal displacements are directed towards the excavation centre. However, to bypass the shortcomings of such empirical assumptions, an analytical approach is proposed to estimate ω_{an} since the constraining angle depends not only on position but also on excavation depth and width-to-length excavation ratio (as demonstrated later in the text).

2.3 *Analytical model for the constraining angle ω_{an}*

The versatility of AC-InSAR deformation analysis lies in its ability to incorporate a kinematic constraint (i.e. $\omega_{x,an}$) derived from analytical models accounting for the excavation and support conditions. In this study, $\omega_{x,an}$ is obtained from a ground loss-based analytical model, described herein. This ground loss approach is chosen to ensure simplicity and uniqueness in the definition of the kinematic constraints, given the inherent complexity of the soil–structure interaction.

An analytical model based on cavity contraction theory is used to estimate $\omega_{x,an}$. The model builds on the work of Zheng et al. (2023), extended here to rectangular deep excavations. The ground movement field is generated by simulating distributed ground loss around the retaining walls. Assumptions of the model include: *(i)* the soil is isotropic, homogenous, and incompressible; *(ii)* retaining wall deflections are modelled as a volumetric ground loss distributed along the walls; *(iii)* vertical strips of the wall are discretised as stacks of spherical cavities of equal volume corresponding to the influence zone and the local wall deflection δ; and (*iv*) 3D displacements from each spherical cavity are calculated using the closed-form solution by Pinto and Whittle (2014). A schematic of this approach, including the discretisation into strips and spherical cavity stacks, is shown in Figure 6. The equivalent radius a of each cavity is defined by:

$$a = \sqrt[3]{\frac{3}{4\pi}\delta(z)\Delta S\Delta H} \quad (9)$$

where $\delta(z)$ is the wall displacement at depth z, ΔS is the horizontal spacing between cavities or horizontal discretization, and ΔH is the vertical spacing. The average wall displacement is computed by integrating the displacement over the wall height and dividing it by the total height. A parabolic profile with depth z is assumed for the wall deflection δ, as per Zheng et al. (2023); however, more realistic wall deflection models can be readily implemented. At each spatial location (x, y, z), the model outputs the displacements $\boldsymbol{u}_{loc,an} = [u_{x,an}\ u_{y,an}\ u_{z,an}]^T$ in the local coordinate system (see Figure 5). From this analytical displacement field, the constraining angle $\omega_{x,an}$ with respect to the local x-axis (aligned with excavation boundaries) is computed as follows

$$\omega_{x,an} = \tan^{-1}\left(\frac{u_{y,an}}{u_{x,an}}\right) \quad (10)$$

These ω_x values define the expected local displacement direction and serve as the input constraint for the decomposition of LOS observations into 3D displacements. This method offers a physically informed alternative to empirical assumptions used in prior studies, such as ω directed towards the centre.

Figure 7 compares the analytically derived $\omega_{x,an}$ from Eq. (10) with the values of $\omega_{x,emp}$ obtained by assuming that the total $\boldsymbol{u}_{h,loc}$ points towards the centre of the excavation. Spatial coordinates are normalised by the depth to limestone ($H_w = 19$ m for SKP). In this way, the constraining angle field $\omega_{x,an}(x/H_w, y/H_w)$ is a function of the shape of the wall deflection δ (assumed parabolic) and is neither affected by magnitude nor by wall depth H_w. In Copenhagen, the extent of ground movement is governed by the thickness of the soil layers ($H_w = H_l\ if\ H_w > H_l$) (Dhanjal et al. 2003).

Both analytical and empirical fields of ω_x are perpendicular to the walls at the central planes of symmetry ($x = 0$ or $y = 0$), as expected. More interestingly, $\omega_{x,an}$ shows a steep rotation in directions around the corners, leading to a more realistic orientation of $\omega_{x,an}$ along the long walls. Also, the two approaches tend to converge at infinite distance from the excavation, as expected for Saint-Venant's principle. Results in Figure 7 illustrate that the empirical assumption could erroneously describe the ground response to deep excavations and, consequently, lead to inaccurate decomposition near corners and edges of the longer walls.

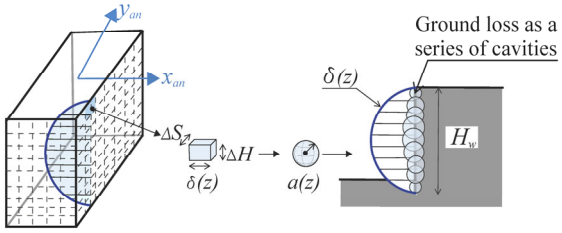

Figure 6. Scheme of the adopted 3D ground loss 3D model.

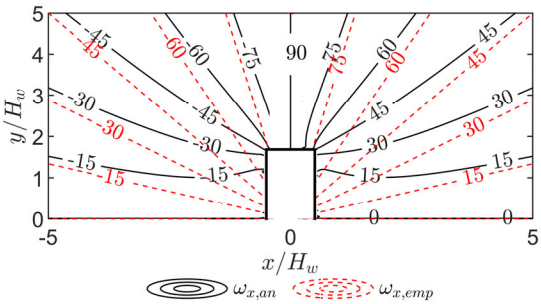

Figure 7. Contours of ω_x: analytical ground loss-based model (solid) versus assumption of orientation towards the centre (dashed).

3 DIRECTIONAL SENSITIVITY OF AC-INSAR ON THE VARIANCE OF LOS MEASUREMENTS

The uncertainty and statistical correlations between the double-orbit LOS measurements and the ground displacements predicted by the AC-InSAR methodology are of interest.

To quantify how errors propagate from the LOS data onto vertical and horizontal displacements, the variance-covariance matrix of $\boldsymbol{u}_\omega = [u_h\ u_z]^T$ and its dependency on the variance of $\boldsymbol{u}_{LOS}$ is analysed. For this, assuming the LOS measurements $u_{LOS,A}$ and $u_{LOS,D}$ are uncorrelated and have identical variance σ_{los}^2 (i.e. distributed noise), the variance-covariance matrix of the constrained displacement vector is

$$\boldsymbol{C} = CoV(\boldsymbol{u}_\omega) = \sigma_{los}^2\left(\boldsymbol{L}_{c,\omega}^T\boldsymbol{L}_{c,\omega}\right)^{-1} \qquad (11)$$

where the diagonal terms C_{vv} and C_{hh} are the variances of the vertical $\sigma_{u,v}^2$ and horizontal $\sigma_{u,h}^2$ displacement components, both proportional to σ_{LOS}^2. Off-diagonal covariance is not considered for the sake of simplicity. From this, the *error amplification factor* is defined as the ratio $\sigma_{u,v}/\sigma_{LOS}$ and $\sigma_{u,h}/\sigma_{LOS}$: the larger this ratio, the higher the propagation of the variance on the LOS measurements onto the expected variance of vertical and horizontal displacements. Thus, elevated error amplification factors can indicate that AC-InSAR is not adequate to measure u_h and/or u_z in a given ω_E, because of the large amplification of LOS variance

Figure 8 displays the error amplification factor obtained for varying constraining angles ω_E in the global coordinate system, based on $\boldsymbol{L}_{c,\omega}$ from Eq. (11) and view angles (CSK descending: $\theta = 26.2°$ and $\alpha = 347.7°$; TSX ascending: $\theta = 42.8°$ and $\alpha = 350.3°$). A peak in error amplification occurs when horizontal displacement aligns with $\omega_E \approx \pm 90°$ (North-South direction), as expected, where the amplification function largely increases. Notably, the variance is higher for horizontal than vertical movements, i.e., $\sigma_{u,h} > \sigma_{u,v}$ across all ω_E, indicating that settlement estimates are more reliable than horizontal ones. This results from the LOS vector being close to vertical, such that u_z contributes more to the LOS deformation than u_E. For instance, for an arbitrary threshold of 5, the orientations are $\omega_E \in [77.5°, 106.5°] + k \cdot 180°$, with $k \in \{0,1\}$for horizontal displacement, while for settlements the interval is $[90°, 94°] + k \cdot 180°$.

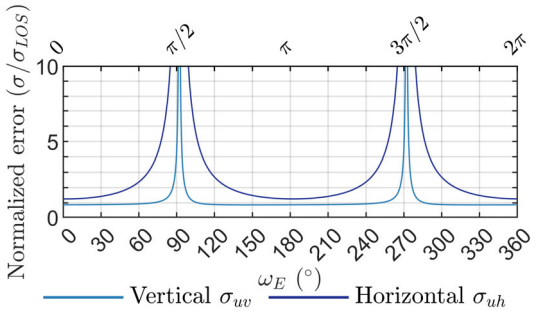

Figure 8. Error amplification factors for u_h and u_z.

4 AC-INSAR AND TERRESTRIAL RESULTS

In this section, MT-InSAR estimates are compared to the 3D target data selected at SKP (Figure 3). At SKP, the local x- and y-axes aligned with the excavation walls have orientation $\beta_a = -44°$ (clockwise from North), see Figure 5. Figure 9(a) shows the temporal evolution of $\omega_{x,field}$ at the 3D target along with the corresponding analytical value $\omega_{x,an} = 11.9°$, while Figure 9(b) shows the magnitude of the total displacement recorded at the target. Furthermore, Figure 10 compares AC-InSAR and 3D target displacements when adopting as an analytical constraint either $\omega_{x,an} = 11.9°$ or the temporal evolution of $\omega_{x,field}$. Note that the AC-InSAR analysis period was limited to the temporal duration of the (shorter) acquisition timeline of the CSK dataset.

During piling, the direction fluctuated between approximately $-50°$ and $50°$, as reported by data in Figure 9(a) while the magnitude of the local total displacement ($\|u_{loc,target}\|$) was negligible (Figure 9(b)). As construction progressed (see stage being indicated with vertical dashed line), the displacement magnitude increased while $\omega_{x,field}$ stabilised around an average of $\omega_{x,field} = 11.5°$ (giving $\omega_{E,field} \approx -32.5°$), which is close to the analytically predicted $\omega_{x,an} = 11.9°$. This confirmed u_h is nearly aligned with the local x-axis towards the excavation and the ground loss analytical model could realistically estimate ω_x.

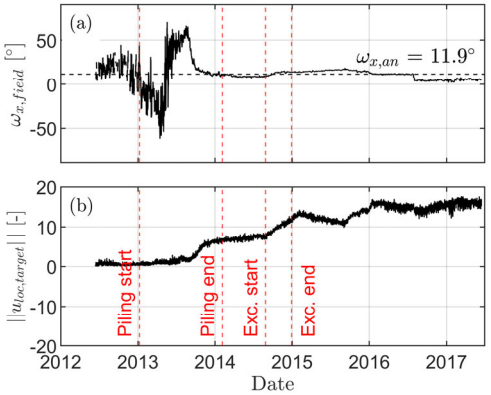

Figure 9. Temporal evolution for the 3D target: (a) angle to the x-axis and (b) magnitude of the total displacement.

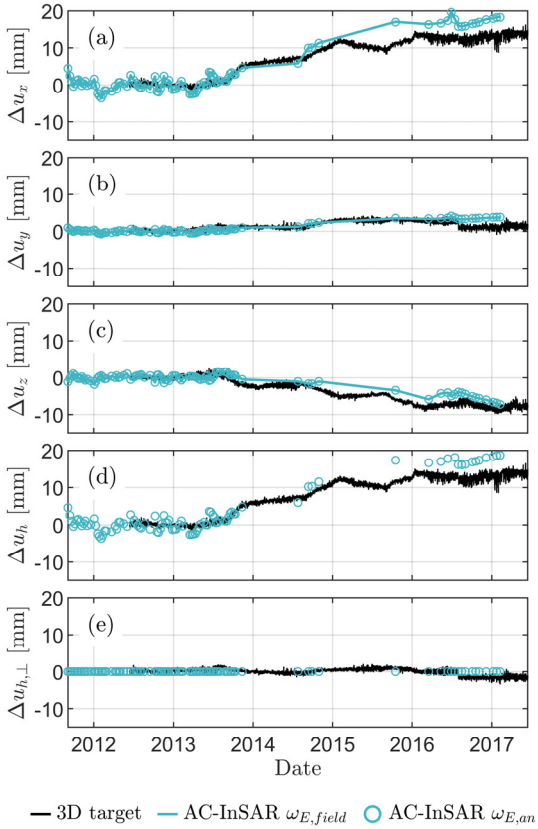

Figure 10. Comparison of AC-InSAR with terrestrial benchmark in the local reference system (a-c) and constrained plane (d and e).

Next, fixing a constraint plane oriented by $\omega_E = \omega_{E,an} = \beta_a + 11.9°$, the AC-InSAR analysis method is evaluated in terms of data for the local displacements $\boldsymbol{u}_{loc}$ with components u_x, u_y and u_z (which are in the directions longitudinal and transverse to the nearby wall along with settlements), in addition to horizontal displacement within the kinematic constraint plane, u_h, and the transverse component to such a plane $u_{h\perp}$ (which is null by assumption for AC-InSAR while it correlates to a measure of the error for the terrestrial dataset). The excellent agreement between the AC-InSAR-derived and target-derived vectors confirms that the proposed methodology effectively captured the salient features of both vertical and horizontal deformation at the specific location, with a non-trivial component of displacement along the wall (u_y) and displacement transverse towards the wall (u_x) greater than the settlement (u_z) of the area close to the target.

5 CONCLUSIONS

This study addressed the AC-InSAR approach that leverages geotechnical knowledge of the excavation problem (namely, the analytical relationship between ground losses and features of the displacement pattern) to reduce the uncertainties in the 3D decomposition of InSAR LOS measurements into vertical and horizontal displacement fields. This approach does not require fixing vertical-to-horizontal movement ratios, which are critical quantities for risk assessments and back-analyses; rather, it introduces an analytically derived field for the horizontal displacement direction (quantified by the angle ω).

The case study at Skjolds Plads (SKP) metro station highlighted the limitations of single-orbit InSAR in deep excavations. At a location of one-quarter of the wall length from the corner, the terrestrial displacement vector was nearly orthogonal to the CSK LOS, rendering CSK effectively "blind". In contrast, while TSX successfully captured the displacement thanks to its favourable viewing geometry, its 3D decomposition still depends on empirical assumptions regarding vertical and horizontal movement. This demonstrates the value of double-orbit MT-InSAR for deep excavation cases when horizontal movements are relevant.

Analytical results illustrated that the complexity of the constraining ω_{field} can be captured with relatively simple analytical models, having as input solely the ground loss distribution at the excavation periphery. Validation of the proposed double-orbit AC-InSAR with terrestrial data confirmed high accuracy: the analytically derived ω differed from field measurements by less than 0.5°, and predicted displacements in both vertical and horizontal directions (perpendicular and longitudinal to the wall) closely matched total station data (see Figure 10). Finally, an error amplification factor to quantify potential "blind" orientations was provided, which requires further investigation.

For practical applications, empirical double-orbit approaches with fixed displacement direction may suffice under plane strain or axisymmetric conditions, such as steady-state tunnelling, circular shafts, or linear excavations. However, this study highlights the value of analytically derived, mechanics-based constraints in InSAR analyses of 3D excavations.

Future work will apply the AC-InSAR method to other Cityringen stations to evaluate its robustness across varied excavation geometries and different relative positions around the excavation perimeter.

6 ACKNOWLEDGEMENTS

The authors gratefully acknowledge Metroselskabet for providing the monitoring data and Innovation Fund for financial support (grant no. 3129-00079B). Note that the content of this paper shall not be considered endorsed by Metroselskabet. The authors would also like to thank the Italian Space Agency for providing COSMO-SkyMed acquisitions under proposal Project ID 1005 METRO-COP and Klimadatastyrelsen for providing the TSX data.

REFERENCES

Brouwer, W.S., and Hanssen, R.F. 2023. A treatise on InSAR geometry and 3-D displacement estimation. *IEEE Trans Geoscience and Remote Sensing* 61:1–11.

Brouwer, W.S., and Hanssen, R.F. 2024. Estimating three-dimensional displacements with InSAR: the strapdown approach. *Journal of Geodesy* 98,110.

Chang, L., Dollevoet, R., and Hanssen, R.F. 2018. Monitoring Line-Infrastructure with multisensor SAR interferometry: products and performance assessment metrics. *IEEE Journal of Selected Topics in Applied Earth Observations and Remote sensing* 11(1), 134–147.

Cascini, L., Fornaro, G., and Peduto, D. 2010. Advanced low- and full-resolution DInSAR map generation for slow-moving landslide analysis at different scales. *Engineering Geology* 112, 29–42.

De Luca, M., Russo, G., Nicotera, M.V., Di Martire, D., and Esposito, I. 2024. A comparison between traditional and satellite monitoring by means of DInSAR technique within the framework of the construction of Metro Line 1 in Naples. *Proc. ICTG 2024*, Vol. 1, 51–62.

Dhanjal, H., Thurlow, P., and Bailey, R. 2003. Building settlement on the Copenhagen Metro project. *In: CIRIA SP201 – Response of Buildings to Excavation-Induced Ground Movements*. London

Fornaro, G., Lombardini, F., Pauciullo, A., Reale, D., Viviani, F. 2014. Tomographic processing of interferometric SAR data: developments, applications, and future research perspectives. *IEEE Signal Processing Magazine*, 31 (4), 41–50.

Giardina, G., Milillo, P., DeJong, M.J., Perissin, D., and Milillo, G. 2019. Evaluation of InSAR monitoring data for post-tunnelling settlement damage assessment. *Structural Control and Health Monitoring* 26(2), e2285.

Noviello, C., Verde, S., Zamparelli, V., Fornaro, G., Pauciullo, A., Reale, D., Nicodemo, G., Ferlisi, S., Gullà, G., and Peduto, D. 2020. Monitoring buildings at landslide risk with SAR: a methodology based on the use of multipass interferometric data. *IEEE Geoscience and Remote Sensing Magazine* 8(1), 56-73.

Olbekk, E., Rocchi, I., Petrella, F., and Grimal, A.C. 2022. Probabilistic back analysis of a Copenhagen metro station. *Proc. 20th International Conference on Soil Mechanics and Geotechnical Engineering, Sydney*. 1-6.

Peduto, D., Korff, M., Nicodemo, G., Marchese, A., Ferlisi, S. 2019. Empirical fragility curves for settlement-affected buildings: analysis of different intensity parameters for seven hundred masonry buildings in The Netherlands. *Soils and Foundations* 59, 380–397.

Peduto, D., Nicodemo, G., Luongo, D., Borrelli, L., Reale, D., Ferlisi, S., Fornaro, G., Gullà, G. 2025. Multi-source data-based quantitative risk analysis of road networks to slow-moving landslides. *Engineering Geology* 350, 108011:1-27.

Pinto, F., and Whittle, A.J. 2014. Ground movements due to shallow tunnels in soft ground. I: analytical solutions. *J. Geotech. Geoenviron. Eng.* 140(4), 04013040.

Ritter, S., Frauenfelder, R., and Vöge, M. 2021. Satellite-based monitoring of urban deep excavations. *Proc. IEEE IGARSS 2021, Brussels,* 1974-1977.

Solarte, E.A.C., Reale, D., Sansosti, E., and Fornaro, G. 2025. Linear and planar projections of DInSAR multi-orbit displacement measurements: general formulation and application to landslides. *IEEE Transactions on Geoscience and Remote Sensing, 63, 1-13.*

Styrelsen for Dataforsyning og Effektivisering. 2022. *Landbevægelser beregnet ud fra TerraSAR-X-satellitdata*. København: SDFE.

Zheng, C., Franza., and Jimenez, R., 2023. Analytical prediction of ground movements due to circular shaft construction in clayey soils. *Canadian Geotechnical Journal*.